Journal of Hydrology 630 (2024) 130631

Contents lists available at ScienceDirect

Journal of Hydrology

journal homepage: www.elsevier.com/locate/jhydrol

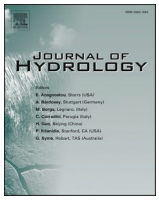

Research papers

Investigating the enigma of an irregular groundwater age pattern in a confined, presumed "fossil" complex aquifer through mixing cell flow modeling

Betzabe Atencio [a], Roi Ram [a,b,1], Avihu Burg [b], Reika Yokochi [c], Yoseph Yechieli [a,b], Roland Purtschert [d], Zheng-Tian Lu [e], Wei Jiang [e], Zeev Ronen [a], Eilon M. Adar [a,*]

[a] Zuckerberg Institute for Water Research, The Jacob Blaustein Institutes for Desert Research, Ben-Gurion University of the Negev, Sde Boker Campus 8499000, Israel
[b] Geological Survey of Israel, 32 Yeshayahu Leibowitz St., Jerusalem 9692100, Israel
[c] Department of the Geophysical Sciences, The University of Chicago, 5734 S. Ellis Ave., Chicago, IL 60637, U.S.A
[d] Climate and Environmental Physics, Physics Institute, University of Bern, Hochschulstrasse 6, Bern 3012, Switzerland
[e] Hefei National Laboratory, School of Physical Sciences, University of Science and Technology of China, Hefei 230026, China

ARTICLE INFO

This manuscript was handled by Corrado Corradini, Editor-in-Chief, with the assistance of Dongmei Han, Associate Editor

Keywords:
Mixing Cell Modeling
Kr-81 groundwater age
Complex aquifer
Nubian Sandstone Aquifer

ABSTRACT

Significant fluctuations in the groundwater (GW) age along the eastern flow path of the Nubian Sandstone Aquifer's (NSA), as derived from Krypton-81 groundwater dating, have suggested that this aquifer, located in Israel's Negev Desert and previously presumed to be a fossil, is not entirely isolated but mixes with younger and even recent water. The intermittent rejuvenation and drastic increases in the GW age across short distances most likely imply hydraulic connectivity with the surrounding aquifers, which contribute both younger and more ancient water to the NSA. The current study aims at modeling the GW flow system to locate and quantify its water sources despite the aquifer's hydrogeological complexity and the scarcity of hydrological data. We implemented the Mixing Cell Modeling (MCM) approach, understanding that the alternating rejuvenations and increases in the GW age downstream of the NSA's eastern flow trajectory reflect the mixing of the NSA's groundwater with young and old GW bodies, respectively. Thus, prompted by the ^{81}Kr water age distribution, yet independent of the Kr radioisotope data, a multi-tracer mixing cell flow model was adopted based on a set of balance equations of water, dissolved minerals, and stable environmental isotopes. The findings indicate that (1) there is a small, yet substantial, intrusion of old brackish GW from a deep-seated, highly pressurized aquifer into the NSA in the northeastern Negev; (2) the rejuvenation of GW in the NSA is due to significant mixing with water from nearby overlying carbonate and chert aquifers, and (3) the NSA is substantially replenished through the Nubian Sandstone (NS) outcrops along the Negev Desert anticlines. Most GW intrusions into the NSA occur near the intersections of the eastern flow path with some of the Negev's major faults and synclines, such as the Paran and Ramon Fault zones and the Zin Syncline. In light of the relatively young GW age at the end of the NSA's western flow path in the northern Negev, and based on the similarities in the hydrogeological structures in the Negev and northern Sinai Deserts, we propose that similar mixing processes with GW from the overlying carbonate aquifers and direct GW recharge through the NS outcrops also occur in the northern Sinai Peninsula. The approach presented in this study might apply to examining recharge processes and hydraulic connectivity in other aquifers that were formerly classified as "fossil," such as the immense NSA found in the Arabian (Jordan & Saudi Arabia) and the Western (Egypt) Deserts.

* Corresponding author at: The Zuckerberg Institute for Water Research, The Jacob Blaustein Institutes for Desert Research, Ben-Gurion University of the Negev, Sde Boker Campus 8499000, Israel.
E-mail address: eilon@bgu.ac.il (E.M. Adar).
[1] Now at the Institute of Environmental Physics, Heidelberg University, Heidelberg 69120, Germany.

https://doi.org/10.1016/j.jhydrol.2024.130631
Received 29 June 2023; Received in revised form 28 November 2023; Accepted 3 December 2023
Available online 19 January 2024

1. Introduction

The deep Nubian Sandstone Aquifer (NSA), under the Sinai (Egypt) and the Negev (Israel) Deserts, has previously been described as a confined, mostly fossil aquifer with negligible active recharge (e.g., Issar, 1979; Issar, 1985; Issar et al., 1972). Groundwater (GW) dating with the ^{14}C radioisotope (half-life of 5730 years) across the confined NSA revealed low ^{14}C activities (<5 pmC), indicating an almost homogeneous ^{14}C age distribution of about 30 kyr (thousands of years) in most of the aquifer, suggesting a significant recharge event during that wetter climate period (e.g., Abouelmagd et al., 2014; Gat and Issar, 1974; JICA (Japan International Cooperation Agency), 1999; Vengosh et al., 2007). Others (Burg et al., 2013) have suggested that such low ^{14}C activities may indicate that most of the NSA waters' ages are older than

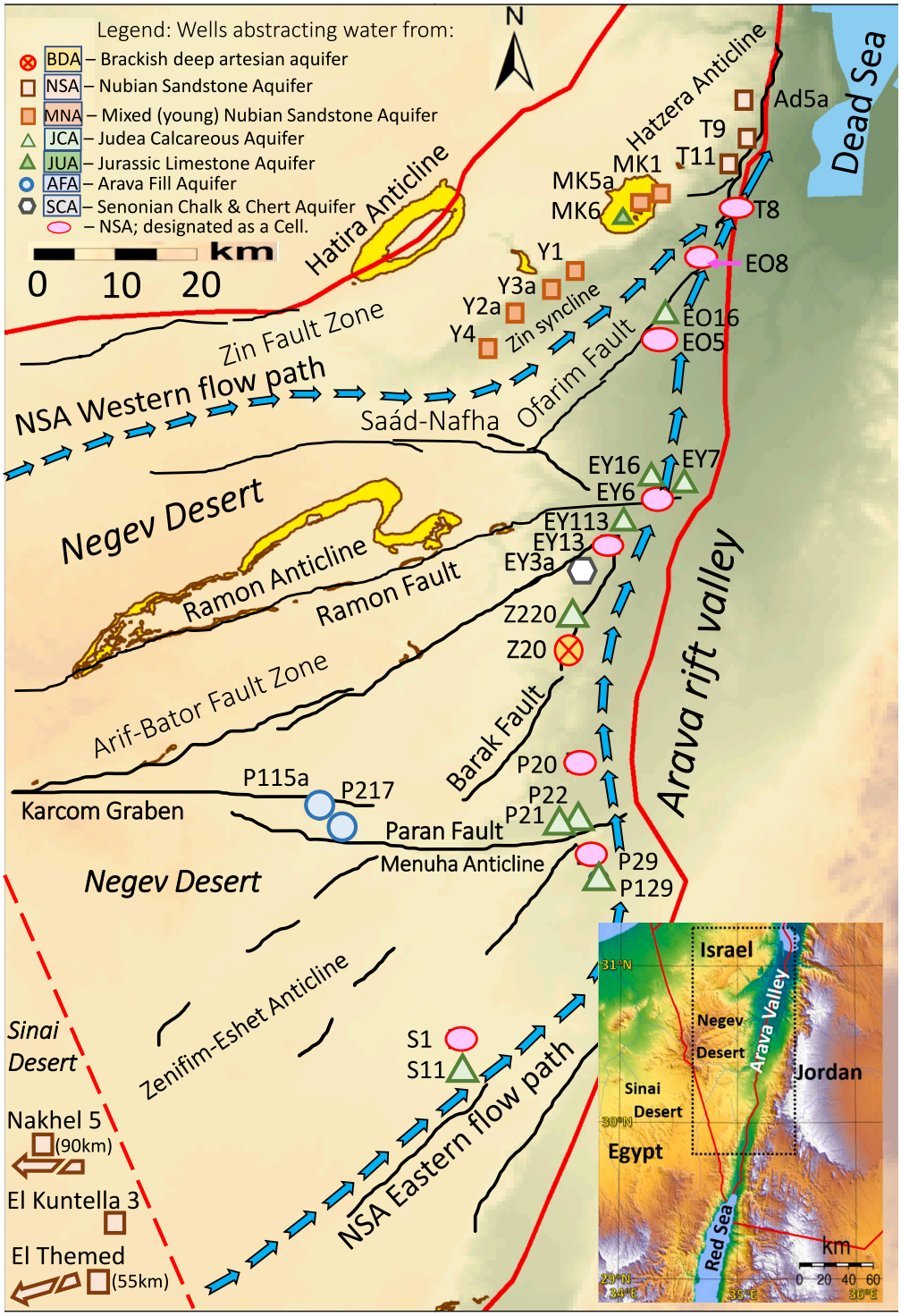

Fig. 1. An orientation map showing: (1) The location of the boreholes from which the groundwater's chemical and isotopic compositions, used in the flow model, were measured. (2) The routes of the two main groundwater flow paths in the Nubian Sandstone Aquifer through the Negev Desert towards the Arava Valley. (3) The geological faults, ridges, and synclines in the Negev Desert and the Arava Valley. (4) The boundary of the Nubian Sandstone Aquifer (red line). (For interpretation of the references to colour in this figure legend, the reader is referred to the web version of this article.)

25 kyr. Based on the small amount of precipitation over the limited NSA exposures in this hyper-arid area over the past half-century, the NSA has been considered to contain "fossil" water, with the understanding that the current recharge rates are negligible, relative to the large reservoir capacity and long residence time (Issar et al., 1972; Ram et al., 2021a, b; Tsur et al., 1989).

The spatial hydraulic gradients suggest two major GW flow paths from the NSA exposures in southern Sinai toward the primary discharge zone south of the Dead Sea (Guttman et al., 1999; Issar et al., 1972; Rosenthal et al., 2007). A western GW flow path runs northward from the NSA's exposure belt in southern Sinai through central Sinai and the northern Negev, while the eastern flow path runs along the eastern edge of the aquifer in the Negev bordering the Arava Rift Valley (Fig. 1). Historical ^{14}C data in the 1 to 10 pmC range, obtained by direct precipitation methods, should be re-evaluated to rule out atmospheric contamination that may have led to an erroneous calculation of the GW age (Aggarwal et al., 2014). The low ^{14}C activities in the GW throughout the Negev and Sinai Deserts (<5 pmC) and the pronounced overall hydraulic gradients of 0.75 to 1.5 per mil along these flow paths contradict the previously assumed relatively homogeneous GW age derived from ^{14}C dating since the GW age is expected to increase downstream in the NSA. This was recently confirmed by GW dating with the ^{81}Kr radioisotope (half-life of 229 kyr) along the NSA's northeastern section, where in most cases, the GW age is beyond the ^{14}C dating capability (Yokochi et al., 2019; Ram et al., 2020).

Contrary to what is expected from an essentially confined and isolated aquifer, the GW age along the eastern Negev flow path does not increase monotonically (Fig. 1). The GW age, deduced from ^{81}Kr, varies from 295 ± 17 kyr in the S1 well to about 360 kyr (376 ± 21 kyr in P29 and 351 ± 14 kyr in P20) 30 km downstream in the Paran area. Further from the Paran area (P wells; Fig. 1), and only 15 km downstream towards the Z20 well, the GW age suddenly increases significantly to 627 ± 47 kyr. A natural gradual GW aging process cannot explain such a drastic increase in GW age, as the flow velocity in the NSA is estimated at

Table 1
The hydrochemical and isotopic composition of groundwater in boreholes constituted the Mixing Cell Model.

Well, (name)	ID	Aquifer¤	Type	^{81}Kr age* (kyr)	EC (mS/cm)	SO_4 (mg/L)	HCO_3 (mg/L)	Na (mg/L)	K (mg/L)	Ca (mg/L)	Mg (mg/L)	TDS (mg/L)	$\delta^{18}O$* (‰)	$\delta^{2}H$* (‰)
Shizafon 1	S1	NSA	Cell I	295±17	3.6	982	209	293	33	340	117	2501	−8.4	−56.8
Paran 29	P29	NSA	Cell II	376±21	3.7	749	224	341	29	278	116	2392	−8.4	−56.1
Paran 20	P20	NSA	Cell III	351±14	3.4	610	204	345	31	275	93	2235	−8.01	−52.11
Ein Yahav 13	EY13	NSA	Cell IV	249±14	3.7	550	256	410	36	260	106	2353	−8.0	−50.7
Ein Yahav 6	EY6	NSA	Cell V	118±14	3.1	561	320	320	25	216	93	2011	−7.6	−46.8
Ein Ofarim 5	EO5	NSA	Cell VI	153±16	3.1	470	326	374	25	200	79	1987	−7.2	−41.2
Ein Ofarim 8	EO8	NSA	Cell VII	204±12	3.2	526	277	332	24	213	79	1966	−7.2	−42.4
Tamar 8	T8	NSA	Cell VIII	236±14	3.4	640	270	377	29	235	74	2170	−7.5	−45.2
El Themed 1[#]	El Themed 1	NSA	source	–	3.5	606	342	466	37	200	161	2240	−6.4	−43.4
El Themed 2[+◦]	El Themed 2	NSA	source	–	–	419[+]	335[+]	262[+]	12.5[+]	157[+]	88[+]	1720◦	−7.7◦	−52.3
El Kuntella 3[ᵃ◦]	El Kuntella 3	NSA	source	–	–	511ᵃ	254ᵃ	193ᵃ	23.4ᵃ	284ᵃ	68.7ᵃ	1827◦	−8.85◦	−63.1◦
Nakhel 5[#]	Nakhel5	NSA	source	–	2.2	286	221	200	18	225	112	1408	−8.76	−57.9
Shizafon 11	S11	JCA	source	222±20	3.2	960	354	317	45	343	129	2614	−7.5	−47.5
Paran 21	P21	JCA	source	91±13	2.8	554	348	224	32	249	94	1839	−7.4	−46.1
Paran 22	P22	JCA	source	–	2.2	553	283	183	21	184	89	1500	−6.6	−39.5
Paran 115a	P115a	AFA	source	<40	1.8	413	238	153	7	163	60	1202	−6.1	−34.2
Paran 129	P129	JCA	source	66±12	4.1	1375	336	290	33	402	209	3057	−7.4	−47.4
Paran 217	P217	AFA	source	–	1.8	380	266	129	7	137	68	1097	−5.7	−31
Ein Ofarim 3	EO3	NSA	source	–	3	467	280	344	20	188	75	1877	−7.3	−42.2
Ein Ofarim 16	EO16	JCA	source	50±12	4.8	654	312	500	25	292	144	2934	−6.5	−36.4
Ein Ofarim 18	EO18	JCA	source	62±12	4.6	538	353	617	31	255	140	2928	−6.6	−36.7
Ein Yahav 3a	EY3a	SCA	source	<40	2.2	522	350	147	13	190	83	1407	−6	−33.3
Ein Yahav 7	EY7	JCA	source	118±14	3.2	565	284	317	25	209	102	2008	−7	−42.3
Ein Yahav 16	EY16	JCA	source	–	3.3	536	293	354	23	210	109	2234	−6.88	−40.8
Ein Yahav 113	EY113	JCA	source	–	1.2	282	214	108	7	83	43	774	−5.5	−27.2
Ein Yahav 116	EY116	SCA	source	42±11	2.5	580	321	251	16	175	89	1658	−6.6	−38.2
Makhtesh 1	MK1	MNA	source	<40	2.4	745	127	217	18	204	75	1621	−5.3	−27.0
Makhtesh 5a	MK5a	MNA	source	<40	3.7	1080	185	413	28	271	117	2574	−5.9	−35.2
Makhtesh 11	MK11	MNA	source	113±9	2.9	358	301	375	22	131	60	1723	−6.7	−35.2
Makhtesh 3	MK3	MNA	source	99±14	3.4	411	285	435	23	155	71	2010	−6.5	−34.3
Makhtesh 6	MK6	JUA	source	421±24	3.8	1232	244	323	30	472	72	2820	−7.8	−48.9
Yorkeam 1	Y1	MNA	source	66±17	3.5	443	300	485	26	161	78	2155	−6.3	−30.8
Yorkeam 2a	Y2a	MNA	source	95±13	2.7	333	287	327	21	134	60	1595	−6.5	–32.5
Yorkeam 4	Y4	MNA	source	46±16	3.1	372	322	400	21	147	70	1856	−6.3	−31.1
Zofar 20	Z20	BDA	source	627±47	10.2	830	254	1370	87	1054	57	7237	−8.4	−56.2
Zofar 220**	Z220	JCA	source	142±16	2.5	555	343	177	30	206	107	1644	−7.1	−43.4
Zofar 24	Z24	SCA	source	<40	2.1	527	364	164	14	189	88	1424	−6.2	−35.8

¤NSA: Nubian Sandstone Aquifer; JCA: Judea Calcareous Aquifer; AFA: Arava Fill Aquifer; SCA: Senonian Chalk Aquifer; MNA: Mixed (young) Nubian Sandstone Aquifer; BDA: Brackish deep artesian aquifer; JUA: Jurassic Aquifer.

*^{81}Kr ages and stable isotope composition after Yokochi et al. (2019), Ram et al., (2020), and Ram et al., (2021b)

**New analyses performed in this study. 81Kr age was computed based on the measured 81Kr activity of 65 ± 3 % of modern atmospheric krypton, measured using the Atom Trap Trace Analysis technique. ^{2}H and ^{18}O isotopes were measured using the Cavity Ring-Down Spectroscopy technique, with a measurement error of 0.5 and 0.1 ‰, respectively.

[#]Well in Sinai. After Abd El Samie and Sadek, 2001. [+] Well in Sinai. After JICA (Japan International Cooperation Agency), 1999.

◦Well in Sinai. After Abouelmagd et al., 2014. ᵃ Well in Sinai. After Abouelmagd, (2012).

0.3–0.7 m per year (Ram et al., 2020). The aforementioned drastic increase in GW age downstream in the aquifer was attributed to mixing with a deep-seated, ancient, saline, pressurized body of water (Ram et al., 2020). Further on, about 25 km to the north, approaching the EY13 well, the GW age suddenly decreases significantly to 249 ± 14 kyr and then further decreases to 118 ± 14 kyr in EY6, 5 km downstream. From here northward, the GW ages gradually increase from 153 ± 16 kyr in EO5 up to 328 ± 28 kyr in Ad5a, with exceptionally younger water in T9 (127 ± 15 kyr), located at the confluence of the far end of the western flow path (Fig. 1), in which much younger GW prevails, from ~ 46 to ~ 95 kyr old (Y1, Y2a & Y4; Table 1). This down-gradient decrease in GW age can only be explained by the GW mixing and diluting with younger water, which is usually accompanied by a significant reduction in salinity. This research aimed to demonstrate the capacity of mixing cell modeling (MCM) to identify and assess GW fluxes of both young, active, and ancient GW sources, such as those that rejuvenate and elevate the GW age in the NSA. We hypothesize that at least along the northern section of the eastern flow path, the NSA gains water from neighboring GW bodies, with both younger and older GW. The objectives were to identify the NSA's active hydraulic connectivity with neighboring aquifers along the eastern flow path and to quantify the GW fluxes from external water-bearing units that possibly intrude into the NSA.

2. Methods

2.1. The challenge

The most common method to address the abovementioned objectives is to fit and calibrate a GW flow model based on the groundwater flow equations (Freeze and Cherry, 1979; Bear, 1979). The NSA's limited hydrological information and its complex hydrogeological structure allowed, at most, the adjustment of a flow model based on continuity equations without the ability to calibrate or verify the model (Guttman et al., 1999; Dvory, 2009. This complex hydrogeological structure and lack of hydrological information pose challenges in implementing a common hydrological numerical flow model that could locate and quantify young or ancient water inflows along the aquifer's eastern flow path. Without sufficient data, these models have a low spatial resolution and are not detailed enough to identify and quantify GW inflows from nearby water bodies. Therefore, the MCM concept was selected as an alternative method for modeling the GW flow system in the NSA in Israel's eastern Negev Desert.

2.2. Mixing cell model

The MCM approach was developed to elucidate complex, unclear GW flow systems (Woolhiser et al., 1982; Campana and Simpson, 1984; Adar et al., 1988; Adar and Neuman, 1988; Bajracharya and Barry, 1994; Partington et al., 2011). It aims to assess the GW fluxes in a complex hydrological system in which the boundaries and hydrological conditions along the boundaries are not well defined or distinct due to a lack of hydrological and hydrogeological information (Matthews, 2013; Wang et al., 2016). Thus, constructing, solving, and calibrating an adequate hydrological numerical flow model based on the continuity approach is not feasible.

It should be noted that GW numerical flow models based on finite differences and finite elements are also compartmental but at more minor scales. Most numerical flow models are based on the flow equations between the cells, while the MCM is based on the mass balance expressions for water and solutes transported with water. Thus, both approaches are equally physically based. While the solution of the flow models is accomplished through numerical analysis of the flow equations between cells, the MCM solution is achieved through a linear or quadratic optimization scheme of mass balance equations (water, solutes, and isotopes) depending on the type (linear or quadratic) of the objective function. The MCMsf (for steady GW flow) computer code is a tool for preparing the input data in an appropriate format for the FORTRAN® solver **Multi.exe** that contains a set of linear hydrochemical balance equations as constraints defining the domain.

Aquifers differ according to the mineral composition of the geological host formations and the groundwater's unique hydrochemical and isotopic characteristics. The mixing of GW from various water-bearing formations depends on GW discharge controlled by the spatial distribution of hydraulic gradients, the permeability of the formations, and the hydraulic connectivity between the aquifers. In light of the GW age and the annual GW abstraction rate relative to the enormous GW reservoir, we assume almost constant GW flow over the vast NSA, although there has been a moderate decrease in the piezometric levels during the last six decades in places with intensive GW abstraction. Therefore, the MCMsf version for a steady flow and steady spatial hydrochemical distribution was selected for this project.

2.2.1. The mixing cell concept

The modeled aquifer was discretized (subdivided) into n homogeneous compartments (cells) within which all the considered parameters, such as hydraulic heads, isotopic composition, and ionic concentrations, are assumed to be constant. All potential unknown fluxes (groundwater fluxes between compartments of the system and discharge of external contributors to the compartments) have been identified and associated with their hydrochemical and isotopic composition.

Regarding the GW hosted in the aquifer for thousands of years, a pseudo-hydrodynamic equilibrium likely prevails between the minerals in the aquifer and the salts dissolved in the water. Therefore, the dissolved minerals constitute only negligible chemical reactions within the aquifer and can be assumed inert for modeling purposes, similar to the water's stable hydrogen and oxygen isotope ratios. However, depending on the local lithological composition (mineralogy) and the climate parameters that prevail in its recharge zone, each source provides a unique water quality.

Drastic spatial and temporal variations in chemical and isotopic composition over short distances within the aquifer are assumed to be exclusively due to variable mixing ratios between the water contributors along the GW flow paths, including a differential contribution from multiple sub-aquifer units. Blending GW from upstream compartments and external sources with existing water in the cell controls the concentrations of the characteristic solutes and the isotopic compositions of each compartment. Complete mixing of all dissolved constituents is assumed within the designated cells. Therefore, every well-mixed or homogeneous aquifer segment is defined as a cell characterized by a unique representative chemical concentration and isotopic composition. No gradients of hydraulic heads, isotopes, or chemical compositions are allowed within the cells, only across the cell's boundaries.

2.2.2. Mathematical description of the MCM for a steady-state flow system

Once the GW flow domain is discretized into homogeneous cells and following the continuum and conservation of mass approach in hydrology (Bear, 1979), a set of mass balance equations for water and the mass flux of solutes is written for each cell n over a given time dt. For aquifers with a constant water density, the mass flux of the water balance for cell n is expressed by:

$$\sum_{r=1}^{R_n} Q_{rn} + \sum_{i=1}^{I_n} q_{in} - \sum_{j=1}^{J_n} q_{nj} - W_n = S_n \frac{dh_n}{dt} \quad (1)$$

where Q_{rn} denotes the water flux (volume/unit time) flowing from R_n different unknown potential sources into cell n, and q_{in} represents the (unknown) water flux from the i^{th} upstream compartment (or cell) into the n^{th} cell. Similarly, q_{nj} stands for the water outflux from the n^{th} cell into the j^{th} downstream cell, and W_n accounts for the known flux of GW abstraction from cell n (i.e., a sink term or pumping rate in the n^{th} cell). The inflows and outflows are iterated over the number of inflows, I_n, and the number of outflows, J_n, associated with every cell n, respectively. S_n

represents the storage capacity within cell n, and h_n denotes the hydraulic head related to that cell. For a steady flow system, the right side of Eq. (1) should be equal to zero, and the water balance expression is written as:

$$\sum_{r=1}^{R_n} Q_{rn} + \sum_{i=1}^{I_n} q_{in} - \sum_{j=1}^{J_n} \overline{q}_{nj} - W_n = \varepsilon_n \tag{2}$$

where ε_n is an error term that accounts for any deviation from zero associated with the water flux balance in cell n, such as an erroneous assessment of the abstracted GW (W_n) or the omission of a hidden influx or outflux of water.

Associated with the water balance, one may combine a mass balance expression for every tracer k out of the total K dissolved constituents in cell n:

$$\sum_{r=1}^{R_n} C_{rnk} Q_{rn} + \sum_{i=1}^{I_n} C_{ink} q_{in} - C_{nk}\left[\sum_{j=1}^{J_n} q_{nj} + W_n\right] = \varepsilon_{nk}\,; (k = 1, 2, \cdots, K \tag{3}$$

where $C_{rk}Q_{rn}$ denotes the k^{th} constituent's average flux [mass/unit time] from source r into cell n, and q_{in} represents the average water flux from the i^{th} upstream cell into the n^{th} cell, having a concentration C_{ink} [mass/volume] of solute k. C_{nk} denotes the concentration of the k^{th} dissolved constituent within cell n, assumed to reflect the weighted average of the influx of the k element by active water fluxes into cell n. ε_{nk} is the error associated with the mass balance of the k^{th} constituent or the deviation from the solute balance in cell n due to possible deviations derived from the water balance and analytical errors in analyzing the isotopic and hydrochemical composition. For every cell, one ends with K + 1 equations: one for the water balance and K more equations for every k species ($k = 1,2,\ldots\ldots, K$) as demonstrated in Eq. (4).

$$\begin{aligned}
&\sum_{r=1}^{R_n} Q_{rn} + \sum_{i=1}^{I_n} q_{in} - \sum_{j=1}^{J_n} \overline{q}_{nj} - W_n = \varepsilon_n \\
&\sum_{r=1}^{R_n} C_{rnk_1} Q_{rn} + \sum_{i=1}^{I_n} C_{ink_1} q_{in} - C_{nk_1}\left[\sum_{j=1}^{J_n} q_{nj} + W_n\right] = \varepsilon_{nk_1} \\
&\sum_{r=1}^{R_n} C_{rnk_2} Q_{rn} + \sum_{i=1}^{I_n} C_{ink_2} q_{in} - C_{nk_2}\left[\sum_{j=1}^{J_n} q_{nj} + W_n\right] = \varepsilon_{nk_2} \\
&\sum_{r=1}^{R_n} C_{rnk_3} Q_{rn} + \sum_{i=1}^{I_n} C_{ink_3} q_{in} - C_{nk_3}\left[\sum_{j=1}^{J_n} q_{nj} + W_n\right] = \varepsilon_{nk_3} \\
&\quad\vdots \quad\quad \vdots \quad\quad \vdots \quad\quad = \quad\quad \vdots \\
&\sum_{r=1}^{R_n} C_{rnK} Q_{rn} + \sum_{i=1}^{I_n} C_{inK} q_{in} - C_{nK}\left[\sum_{j=1}^{J} q_{nj} + W_n\right] = \varepsilon_{nK}
\end{aligned} \tag{4}$$

Upon combining Eqs. (2) and (3) into a matrix form for each cell n, one obtains:

$$\underline{\underline{C}}_n \underline{X}_n + \underline{P}_n = \underline{E}_n \; (n = 1, 2, \cdots, N) \tag{5}$$

where $\underline{\underline{C}}_n$ is a matrix with known concentrations (Eq. (6)), $\underline{X}_n$ is the vector of unknown water fluxes entering and leaving cell n (Eq. (7)), Pn is a vector of the known water abstraction out of cell n (Eq. (7)), and $\underline{E}_n$ is the error vector (Eq. (8)).

$$\begin{vmatrix}
1, & 1, \cdots, & 1, & 1, & 1, \cdots, & 1, & -1, & -1, \cdots, & -1 \\
C_{r_1nk_1}, C_{r_2nk_1}, \cdots, C_{R_nnk_1}, & C_{i_1nk_1}, C_{i_2nk_1}, \cdots, C_{I_nnk_1}, & -C_{nj_1k_1}, & -C_{nj_2k_1}, \cdots, & -C_{nJ_nk_1} \\
C_{r_1nk_2}, C_{r_2nk_2}, \cdots, C_{R_nnk_2}, & C_{i_1nk_2}, C_{i_2nk_2}, \cdots, C_{I_nnk_2}, & -C_{nj_1k_2}, & -C_{nj_2k_2}, \cdots, & -C_{nJ_nk_2} \\
C_{r_1nk_3}, C_{r_2nk_3}, \cdots, C_{R_nnk_3}, & C_{i_1nk_3}, C_{i_2nk_3}, \cdots, C_{I_nnk_3}, & -C_{nj_1k_3}, & -C_{nj_2k_3}, \cdots, & -C_{nJ_nk_3} \\
\vdots\vdots\vdots\vdots\vdots & \vdots\vdots\vdots & \vdots & \vdots & \vdots \\
C_{r_1nK}, C_{r_2nK}, \cdots, C_{R_nnK}, & C_{i_1nK}, C_{i_2nK}, \cdots, C_{I_nnK}, & -C_{nj_1K}, & -C_{nj_2K}, \cdots, & -C_{nJ_nK}
\end{vmatrix} \tag{6}$$

$$\underline{X}_n = \begin{vmatrix} Q_{r1} \\ Q_{r2} \\ \vdots \\ Q_{Rn} \\ q_{i1} \\ q_{i2} \\ \vdots \\ q_{In} \\ q_{n1} \\ q_{n2} \\ \vdots \\ q_{nJn} \end{vmatrix} [(R_n + I_n + J_n)*1] \tag{7}$$

$$\underline{P}_n = \begin{vmatrix} W_n \\ C_{nk_1} W_n \\ C_{nk_2} W_n \\ C_{nk_3} W_n \\ \vdots \\ C_{nK} W_n \end{vmatrix} [(K+1)*1] \tag{8}$$

$$\underline{E}_n = \begin{vmatrix} \mathrm{E}_n \\ \mathrm{E}_{nk_1} \\ \mathrm{E}_{nk_2} \\ \mathrm{E}_{nk_3} \\ \vdots \\ \mathrm{E}_{nK} \end{vmatrix} [(K+1)*1] \tag{9}$$

Based on Eq. (5) and by assembling the square error terms over all N cells, we obtain a quadratic objective function (Eq. (10)):

$$J = \sum_{n=1}^{N} \left[\underline{E}_n{}^T \underline{\underline{\Phi}}\, \underline{E}_n\right] = \sum_{n=1}^{N} \left[\left(\underline{\underline{C}}_n \underline{X}_n + \underline{P}_n\right)^T \underline{\underline{\Phi}}\, \left(\underline{\underline{C}}_n \underline{X}_n + \underline{P}_n\right)\right] \tag{10}$$

^{T} denotes transpose, and $\underline{\underline{\Phi}}\left(0.1 \le \underline{\underline{\Phi}} \ge 1.0\right)$ represents a diagonal matrix comprising weighting values associated with the estimated errors (independent of each other) expected for each tracer, which compose the mass balance of the dissolved constituents. It reflects the degree of confidence with which the tracers are assumed to be conservative in the aquifer and the analytical deviation of the chemical and isotope analyses. With such a quadratic objective function, one can guarantee that only positive values will be assigned to the calculated unknown fluxes in the optimization process.

All identified flux components in the modeled aquifer can now be estimated by optimizing the above quadratic objective function by minimizing the sum of square errors, J, using the *simplex method* of the *Wolfe Mathematical Algorithm* (Wolfe, 1959). The most acceptable solution from the optimization scheme is the set of fluxes calculated for each active flow from those defined as potential flows in vector $\underline{X}$ that provide the lowest error vector $\underline{E}$. In case the computed fluxes entail substantial gaps in water and dissolved chemical balances, one may modify the setup and the proposed flow pattern with the associated hydrochemical and isotopic characteristics until the most feasible solution is obtained.

To run the model, one must insert all the abstracted water fluxes from each cell that composes the P vector. In addition, the water flux out of the last downstream cell should be assessed. The sum of the pumped GW fluxes and the outflow discharging out of the last cell set a firm constraint on the water balance for the optimized solution. The GW in the eastern NSA is presumed to flow from the southern Sinai to the central Negev and further along the margins of the Arava Valley towards the discharge area south of the Dead Sea (Fig. 1).

2.3. Setting the MCM configuration for the eastern negev nubian sandstone aquifer

The hydrochemistry and isotopic compositions of eight wells along the NSA's eastern flow path were selected to designate "cells" along this flow path. The technical information for these wells indicates that the screens are located within the sandstone formation, and massive mechanical sealings (cement and clay around the production pipe in the borehole) avoid leakage through the borehole's annulus from the overlying calcareous aquifer. Thus, the GW pumped out of these wells represents, with high probability, the NSA's local chemical and isotopic composition without mixing with the overlying aquifer. The schematic GW flow pattern and the wells representing potential contributors from the surrounding aquifers are presented in Fig. 2. Following the significant hydrochemical and isotopic variations, each of the wells along the eastern flow path was chosen to represent a "homogeneous cell" except at the northern end of the flow path, where the eastern and western flow paths meet. Following preliminary single-cell MCM tests, the Tamar 8 (T8, Fig. 1) well was selected to characterize the last cell since the upstream NSA's groundwater type strongly influences its hydrochemical and isotopic composition. The GW in the nearby Tamar 9 and 11 wells seems to be strongly influenced by mixing with the NSA's western flow path through the nearby fault zone. Each cell was assigned its characteristic hydrochemistry, isotopic composition, the total annual amount of abstracted GW, and designated wells from neighboring water-bearing formations that might (potentially) mix with the NSA at this location. With a lack of more accessible boreholes, several external sources were considered potential contributors to more than one cell. The GW abstraction rates are the known fluxes in the above water, chemical, and isotopic balance expressions. The annual GW pumping rates were obtained from the Israel Water Authority for all production wells within each cell (designated by blue arrows in Fig. 2). The GW discharge at the outlet of the aquifer toward the Dead Sea Basin was initially assessed at about 12.4 Mm^3/y, following Guttman et al. (1999).

Nine parameters, including six major ions (SO_4, HCO_3, Ca, Mg, Na, K), total dissolved solids (TDS), and ^{18}O and ^{2}H stable water isotopes (Table 1) were used to characterize each cell and every potential contributor. Therefore, following Eq. (4), ten balance equations, including water balance, were written for every cell, with a total of eighty balance equations for the eight compartments covering the entire flow domain.

Direct evidence for young (^{14}C-bearing) GW in the Negev Desert's NSA was obtained only within the northeastern NSA exposures at the Hatzera Anticline (MK wells; Ram et al., 2020), most likely reflecting active GW recharge on the nearby outcrops. The relatively young ^{81}Kr age found in boreholes Y1 to Y4, located towards the end of the western

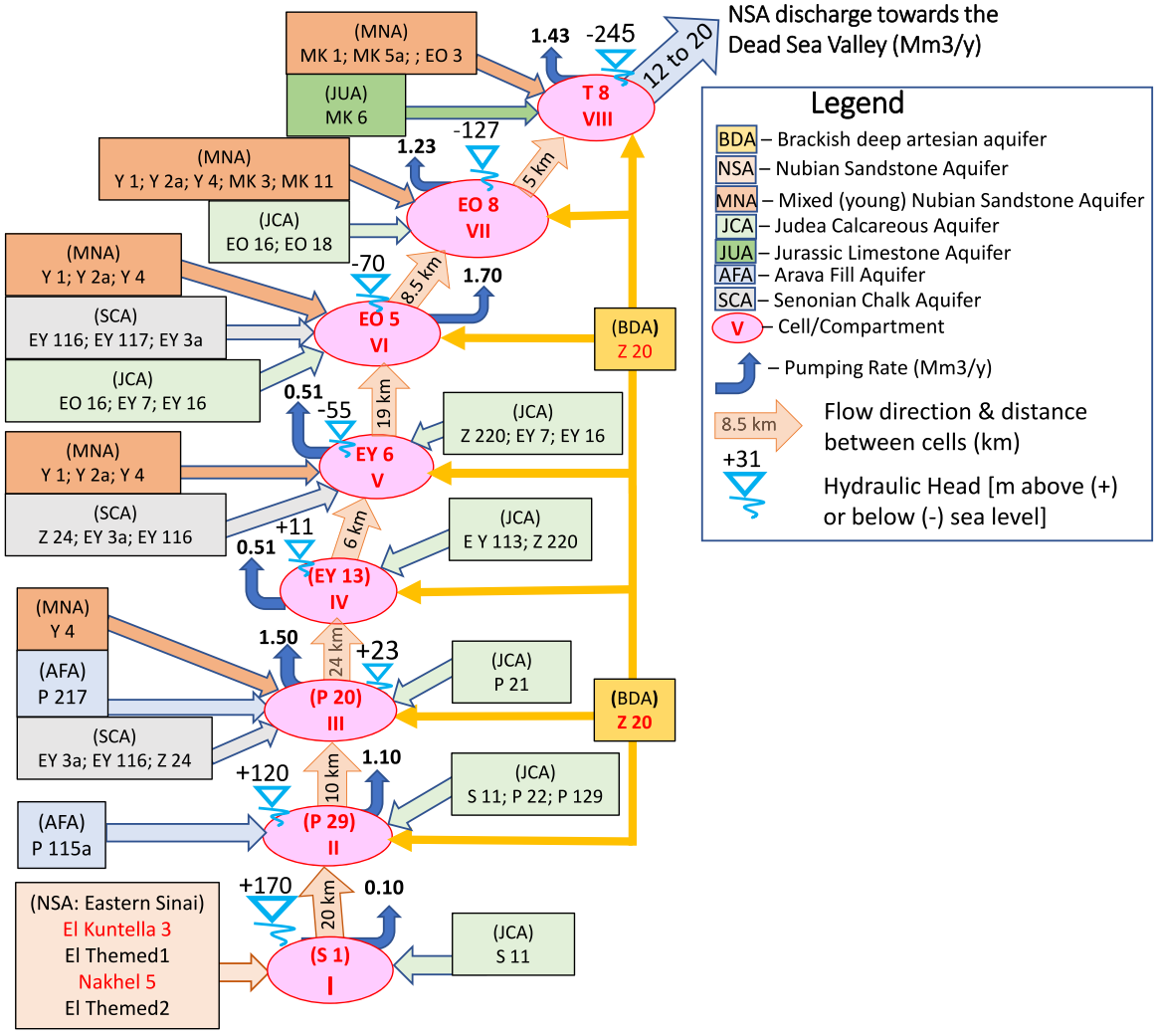

Fig. 2. A schematic setup of the compartmental configuration of the groundwater flow pattern along the eastern Negev flow path of the Nubian Sandstone Aquifer. "Cells" are illustrated as pink circles. Orange arrows denote groundwater fluxes between cells and the assessed outflux, while the known pumping rates are denoted by blue arrows. According to the legend, rectangles with different colors mark the potential contributors to each cell from all feasible sources (aquifers). (For interpretation of the references to colour in this figure legend, the reader is referred to the web version of this article.)

flow path, where one would expect a water age of hundreds of thousands of years, suggests a similar recharge mechanism through the nearby NSA outcrops at the top of the Hatira Anticline (Fig. 1). We also hypothesize that these 800-m-deep boreholes represent the NSA groundwater's hydrochemical and isotopic composition at the far end of the western flow path before it mixes with the eastern flow path in proximity to the Dead Sea outlet. In the absence of observation boreholes within and in proximity to the NSA's outcrops in the Ramon Anticline, for modeling purposes, we assumed that GW with similar hydrochemical and isotopic compositions might have also recharged the NSA through these nearby outcrops located ~ 50 km southwest of the Hatzera Anticline and ~ 20 km west of the eastern flow path (Fig. 1).

3. Findings and results

We applied the MCM to assess 53 feasible unknown GW inflow components from upstream and the surrounding aquifers (Fig. 2), plus seven unknown GW fluxes between the eight cells. Altogether, the potentials of 60 unknown water fluxes were examined with the MCM. The krypton radioisotope activities used to calculate the GW ages were not included in the hydrochemical and isotopic elements used to set the constraints and the objective function of the optimization scheme to avoid any numerical relation between the MCM and the ^{81}Kr water ages.

The calculated GW fluxes for the most feasible scenarios with the lowest water balance error are presented in Table 2 and illustrated in Fig. 3. The most viable runs of the MCM with the lowest water balance error (<1%) found 24 positive external contributors to the modeled NSA. It was determined that most of the error in water balance was caused by a disparity of the flows in the last cell, where the outflow leaving the NSA into the Arava Valley was set at 12.4 Mm^3/y according to the previous estimate (Guttman et al., 1999). Reruns of the model with only the abovementioned positive contributors yielded a water balance error of 0.1 % when the outgoing flow was slightly reduced to about 11.2 Mm^3/y.

The first upstream cell (Cell I), designated by the hydrochemistry and isotopic composition of well S1, is the most southern well in the Negev, abstracting GW from the NSA. As expected, the MCM reveals that it is fed by upstream NS groundwater from central Sinai, defined by the hydrochemistry and isotopes as reported for the Nakhel 5 and El Kuntella 3 wells (0.24 Mm^3/y and 0.15 Mm^3/y, respectively) and by a firm contribution (0.37 Mm^3/y) from the overlying Judea Calcareous Aquifer (JCA) designated by S11, abstracting GW from the lower JCA's water-bearing formations. All the other MCM scenarios rejected El Themed 1 or El Themed 2 (Fig. 2) as positive contributors to the upstream Nubian sandstone-type of water. Almost 0.61 Mm^3/y flowed downstream into Cell II, characterized by P29, under a hydraulic gradient of ~ 2.5 ‰ (Fig. 3).

Beyond the GW outflux from Cell I, an additional 0.37 Mm^3/y of GW enters the NSA in Cell II from the overlying JCA designated by the S11 (0.24 Mm^3/y) and P129 (0.13 Mm^3/y) wells. A substantial additional amount of 0.64 Mm^3/y enters Cell II from the western local Alluvial Fill Aquifer (AFA), characterized by P115a, found in the Karcom Graben (Fig. 1). Following Dvory (2009), the latter fresh GW component probably joins the NSA through the Paran Fault (Fig. 1). Cell II is also fed by a small, yet significant, amount of relatively salty GW leaking upward from the deep-seated, pressurized, brackish GW reservoir discovered in Z20, 1.2 km below the surface. Further downstream, Cell III (designated by P20) is fed by ~ 0.5 Mm^3/y of NS groundwater that comes from upstream (Cell II) and by a significant amount of brackish GW (0.12 Mm^3/y) designated by Z20. The contribution of brackish GW in varying amounts was detected in all cells downstream toward the Dead Sea. In addition, a quantity of GW (0.64 Mm^3/y) from the JCA and an additional amount of 0.17 Mm^3/y (Fig. 3 and Table 2) from the AFA in the Karcom Graben (Fig. 1) are mixed with the NSA groundwater in the Cell III area, which could explain the rejuvenation of the GW age downstream from P29 to P20 (376 kyr vs. 351 kyr in P29 and P20, respectively).

A striking finding is the discontinuity of the GW flow in the NSA observed between Cells III and IV. This is a direct result of the large GW abstraction (~2.6 Mm^3/y) for irrigation in the Paran Basin (Cells II & III), which has lowered the piezometric gradient from ~ 1.5 ‰ to 0.5 ‰ between P20 and EY13, thereby minimizing the GW flow downstream towards the Ein Yahav Basin (Cell IV). Without a substantial GW inflow from the upstream section in the last five decades, the GW currently abstracted from Cell IV (~0.51 Mm^3/y) is supplied by attracting relatively young GW into the NSA from the JCA designated by Z220; this GW has a ^{81}Kr age of only 142 kyr and seems to be diverted into the NSA through the Arif-Bator Fault zone (Fig. 1). This explains the drastic decrease in the GW age from 351 kyr in Cell III (P20) down to 249 kyr in Cell IV (EY13), 20 km downstream.

A minimal water flux discharges from Cell IV into downstream Cell V (designated by EY6) despite a steep piezometric gradient of 11.1 ‰, reflecting the GW abstraction for intensive agriculture in the Cell V area. Three types of relatively young GW from neighboring aquifers seem to be with the NS groundwater in Cell V. These include the JCA, SCA (Senonian Chalk Aquifer), and MNA (Mixed Nubian Sandstone Aquifer, designated by the Y4 GW type), with computed GW fluxes of 3.65, 0.95, and 0.73 Mm^3/y, respectively. This contribution from the eastern Negev aquifers is apparently facilitated through the Ramon Fault zone (Dvory, 2009) that meets the Arava Rift Valley a few kilometers downstream of EY13, near EY6 (Fig. 1) and diverts a substantial amount of relatively young GW (similar to the Y4 GW type) that rejuvenates the NS water from 249 kyr to 118 kyr across only 6 km. The Y4 GW type represents, in the MCM, the GW type at the far end of the NSA's western flow path through central Sinai (Fig. 1). Unlike the end of the eastern flow path, the GW age in the western flow path ranges from 46 kyr to 95 kyr (Y1, Y2a & Y4; Table 1), reflecting the contribution of young GW that

Table 2
Optimized solution for fluxes out of 24 potential sources and their corresponding groundwater contribution (a), and fluxes between the eight cells (b) along the eastern flow path of the Nubian Sandstone Aquifer in the Negev Desert.
(¤Aquifer abbreviations as appear in Fig. 1.)

(a) Cell	Source	Aquifer¤	Flux Mm^3 y^{-1}
Cell I-Shizafon 1	Shizafon 11	JCA	**0.37**
	El Kuntella 3	NSA	**0.15**
	Nekhel 5	NSA	**0.24**
Cell II-Paran 29	Paran 129	JCA	**0.13**
	Paran 115a	AFA	**0.64**
	Zofar 20	BDA	**0.05**
	Shizafon 11	JCA	**0.24**
Cell III-Paran 20	Zofar 20	BDA	**0.12**
	Paran 21	JCA	**0.64**
	Paran 217	AFA	**0.17**
Cell IV-Ein Yahav 13	Zofar 20	BDA	**0.07**
	Zofar 220	JCA	**0.47**
Cell V-Ein Yahav 6	Zofar 20	BDA	**0.07**
	Ein Yahav 7	JCA	**3.65**
	Yorkeam 4	MNA	**0.73**
	Ein Yahav 3a	SCA	**0.95**
Cell VI-Ein Ofarim 5	Zofar 20	BDA	**0.19**
	Ein Yahav 7	JCA	**0.56**
	Yorkeam 4	MNA	**5.49**
Cell VII-Ein Ofarim 8	Zofar 20	BDA	**0.06**
	Ein Ofarim 16	JCA	**0.82**
Cell VIII- Tamar 8	Zofar 20	BDA	**0.52**
	Makhtesh 1	MNA	**2.01**
	Makhtesh 6	JUA	**0.95**

(b)	From Cell	To Cell	Flux Mm^3 y^{-1}
	I	II	0.61
	II	III	0.49
	III	IV	0.00
	IV	V	0.05
	V	VI	4.68
	VI	VII	9.12
	VII	VIII	9.28

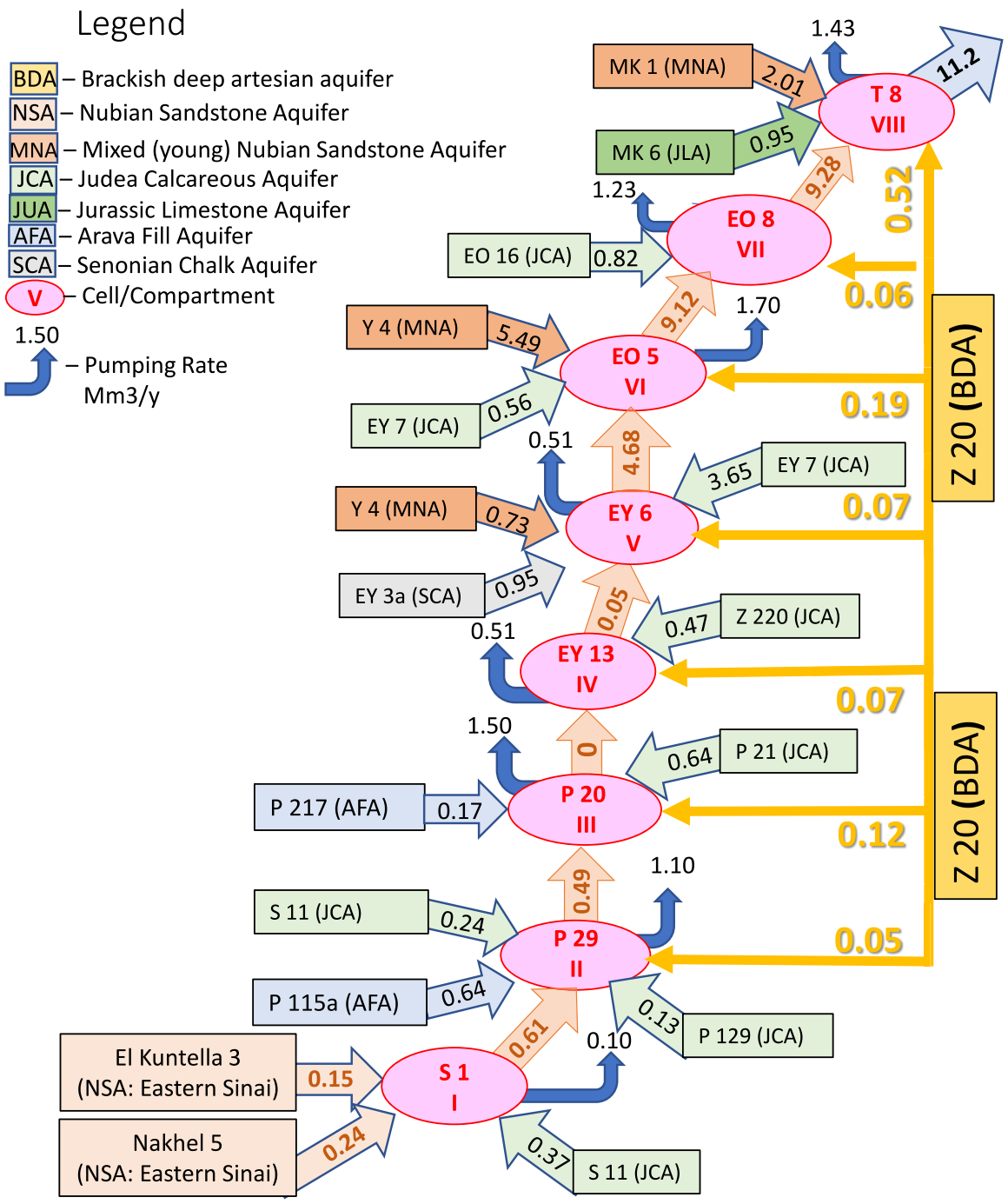

Fig. 3. Calculated groundwater fluxes within the arrows along the Nubian Sandstone Aquifer under the eastern Negev Desert and the designated inflows from neighboring aquifers solved with the MCM (all values are in million cubic meters per year).

recharges the NSA through the NS outcrops over the northeastern Sinai and Negev Anticlines.

According to the MCM results, further to the north in Cell VI (designated by EO5) is where the eastern and western NSA flow paths meet and mix. The MNA type of GW is the primary external source of Cells VI and VIII, with 5.49 and 2.01 Mm^3/y, respectively (Fig. 3). JCA groundwater gets mixed with the NSA in Cells VI and VII, while the carbonated water that flows into Cell VIII (0.95 Mm^3/y) seems to be provided by the underlying Jurassic Limestone Aquifer (JUA). Despite the massive GW abstraction by the Dead Sea Works (1.7, 1.23 & 1.42 Mm^3/y in Cells VI, VII & VIII, respectively), the GW fluxes gradually increase toward the discharge zone from 4.68 to 9.12 and 9.28 Mm^3/y, following a drastic increase of the piezometric gradient towards the Dead Sea Rift Valley, from 0.7 ‰ to 6.7 ‰ and 23.6 ‰ in the last three cells, respectively. Finally, the best optimal solution for the eastern flow path was achieved when the annual outflow from the NSA was determined to be 11.2 Mm^3/y, very close (practically the same) to the quantity of 12.4 Mm^3/y calculated by the northern Negev-Arava GW numerical flow model (Guttman et al., 1999).

4. Discussion

The MCM results (Fig. 3) indicate that the NSA's upstream recharge in the southern Negev is characterized by the El Kuntella 3 and Nakhel 5

water types located in the eastern and central Sinai, respectively. None of the MCM scenarios found that the El Themed well's GW type (Fig. 2), also located upstream of the Negev NSA (Fig. 1), contributes to or feeds the NSA in the southern Negev. The latter wells were drilled south of the Themed Fault, a major E-W fault that crosses the central Sinai Peninsula with a vertical displacement of 400 to 500 m in eastern Sinai (Moustafa and Khalil, 1994; WPRP, 1998). The model's results strengthen the assertion that this major fault forms a hydrogeological barrier between the southern and central NSA across the Sinai Peninsula and channels the GW flow in the NSA toward a hydrogeological opening in the Nakhel area (JICA (Japan International Cooperation Agency), 1999; Shalaby et al., 2012), from where it flows to the northern Sinai and east towards the Negev and the Dead Sea Rift Valley (Figure 1 in Ram et al., 2020).

During the last several decades, the NSA has been presumed to be confined and isolated. Despite the NSA's hydrogeological complexity and the limited hydrological information about it, the MCM allowed us to identify the NSA's hydraulic connectivity to the surrounding calcareous, chalk and chert, and alluvial aquifers. It turns out that despite being confined, the NSA is not entirely isolated. It receives a massive GW inflow in several locations from the surrounding calcareous aquifers along the entire length of its eastern flow path, accompanied by a small yet significant intrusion of brackish water from a deep artesian reservoir.

In several sites along the eastern flow path in the lower edge of the eastern Negev, pairs of production wells were unconnectedly drilled into the NSA and the JCA. In most cases, the hydraulic head in the NSA is higher than in the overlying JCA. For example, the initial hydraulic head in S1 (NSA) was ~ 170 masl (m above sea level) compared to ~ 125 masl in S11 and + 11.5 masl in EY13 (NSA) versus −4 mbsl (m below sea level) in EY113 (JCA), and ~ -55 mbsl in EY6 (NSA) versus -~-62 mbsl in EY16 (JCA). Therefore, despite the MCM results showing a massive GW contribution from the JCA to the NSA, one should not expect the downward leaking of JCA GW into the NSA in these locations as reflected by the apparent differences in the hydrochemical and isotopic compositions (Appendix A: Supplementary Materials: Figs. S.1 & S.2) and the GW age in the two aquifers (Table 1; Burg et al., 2013). It is worth noting that stratigraphic logs, as well as water table measurements, were taken during the drilling of several deep wells in the Negev, suggesting that the impermeable layer separating the NSA from the overlying JCA is a few tens of meters above the Nubian sandstone–Judean limestone interface within the lower section of the JCA (Guttman et al., 1999; Burg et al., 2013). Therefore, the upper section in the NSA and the lower section in the JCA form a united body of GW with both calcareous and sandstone hydrochemical and isotopic affinities (Vengosh et al., 2007; Rosenthal et al., 2007), following the relative GW contribution from each formation in each specific location. Theoretically, this might also explain the MCM results showing the JCA's substantial contribution to the NSA. Although we do not have detailed GW information due to a lack of boreholes across the Negev Highlands, overland flows and erratic floods from desert storms recharge the JCA, as extensive outcrops of the Judea Calcareous formations throughout the Negev Anticlines exceed 600 to 800 masl, due to receiving winter precipitation including snow. The foothills of the eastern Negev ridges are inclined eastward toward the Rift Valley. Therefore, GW drains eastward along the synclines and the Negev' 's latitudinal faults (Fig. 1), penetrating the NSA along the contact plains between the JCA and the NSA in the high Negev Mountains, where the hydraulic heads in the JCA are most likely higher than in the NSA. It is important to note that every attempt to run the MCM, while excluding the JCA type of GW as a potential contributor to the NSA, elevated the error balance. In most cases, it reached an unbounded optimization scheme that did not yield an optimal solution, a fact that supports considerable hydraulic connectivity between the two aquifers.

The NSA's eastern flow path towards the Dead Sea outlet passes under and along the JCA's inclined margins, in which a piezometric head that is lower than that of the underlying NSA prevails. However, the JCA is exposed to GW recharge over vast areas in the Negev Highlands and anticlines west of the Arava Valley. Yet, without wells or observation boreholes across the Negev Highlands, one can assume, with a high probability, that the piezometric heads in the JCA formations along the anticlines are high enough to allow the passage of GW into the NSA, as depicted at the eastern edge of the Zenifim-Eshet and Menuha Anticlines (Fig. 1), where the piezometric head in P129 (JCA) is ~+135 masl versus ~+120 masl in P29 (NSA).

The spatial distribution of the faults across the Negev may explain the GW entry route into the NSA from nearby aquifers. The model results and the location of the P29 and P20 wells (Cells II & III) suggest that the Paran Fault allows the GW from the alluvial aquifer in the Karcom Graben (Fig. 1) to flow into the NSA in the Paran Basin on the edge of the eastern Negev. The Barak and the Arif-Bator Faults seem to divert younger GW from the JCA into Cell IV (EY13), and the Ramon and Saad-Nafha Fault zones shift both MNA and JCA water toward the NSA in Cell V (EY6) and Cell VI (EO5). In addition, the NSA's western flow path approaches the Dead Sea Valley through the synclines between the Hatira, Hatzera, and Ramon Anticlines, providing the northern edge of the eastern NSA with a substantial amount of mixed (older + younger) Nubian sandstone GW.

The MCM estimates the downstream GW fluxes between all segments of the NSA along the eastern flow path. It also identified the limited, if any, GW flows downstream of Cell III, following the massive GW abstraction in the Paran Basin for intensive irrigation. Starting from Cell IV, the GW flow in the NSA increases as it approaches the Dead Sea rift: 0.05 Mm^3/y, 4.68 Mm^3/y, 9.12 Mm^3/y, 9.28, and 11.2 Mm^3/y drain out from Cells IV, V, VI, VII, and VIII, respectively, reflecting the NSA's increasing thickness (Calvo and Gvirtzman, 2013; Kroitoru, 1980) and the rise in the hydraulic gradients, from 0.78 ‰ between Cells V and VI to 6.7 ‰ between Cells VI and VII, and 23.6 ‰ between Cells VII and VIII. Following the massive GW abstraction during the last five decades from the GW basins under Cells II, III & IV, the sources of the downstream fluxes beyond Cell IV mainly stem from the local storage in the NSA, groundwater originating from the western NSA flow path, and GW fluxes out of the calcareous aquifers across the Negev Highlands (JCA and SCA). In the last cell (Cell VIII, T8), located in proximity to the aquifer's discharge zone, about 30 % of the water inflows originate from the Jurassic Limestone Aquifer and not from the Upper Cretaceous JCA. The MCM finding that the MNA water type feeds three cells downstream in the eastern NSA's flow path (Fig. 3) indicates that the western and the eastern flow paths unite towards the aquifer's outlet into the northern Arava Valley, south of the Dead Sea.

Based on mass balance equations of water and solutes, the MCM estimates that the NSA discharges about 11 Mm^3/y towards the Dead Sea Basin, very similar to the outflow of ~ 12 Mm^3/y computed using a numerical flow model based on the flow equation (Dvory, 2009). However, the MCM expands beyond the previous model and also enables to identify and quantify substantial inflows from adjacent aquifers into the NSA along the eastern Negev flow path and the zone where the eastern and western flow paths merge in the northeast Negev Desert before they drain towards the Dead Sea.

The Z20 is a flowing artesian well with brackish water, suggesting at least 126 bars down the borehole, 1.2 km below the surface, drilled into the NSA between the Paran and the Ein Yahav Basins (Cells III and IV). Not only is the GW's age exceptionally ancient (627 kyr, only 15 km downstream of the Paran area where the GW age is around 350 kyr; Ram et al., 2020), but its salinity (EC = 10.2 mS/cm; Table 1), and its hydrochemical composition are significantly higher and entirely different, than the other NSA wells. The documented well's log shows that the borehole crosses a major fault believed to be part of the pronounced Barak Fault (Frieslander, 2000), which, following the MCM results, seems to allow upward leakage of brackish GW into the NSA. Lacking the ability to identify a prominent end member that could account for its hydrochemical composition, the MCM failed to reach a solution for any attempt to include Z20 as a designated cell within the

eastern flow path. Therefore, we excluded Z20 as a cell in the flow model and introduced the Z20 type of GW as a potential source of old brackish GW along the eastern NSA. The MCM result confirms that the Z20 GW type leaks upward into the NSA from an assumed, yet hidden, deep-seated pressurized water-bearing formation along the eastern Negev flow path, starting from the Paran Basin. The salty upward fluxes are relatively small, varying from 0.05 to 0.19 Mm^3/y, except for 0.52 Mm^3/y into the last cell before final discharge into the Dead Sea Basin (Fig. 3). Even though the MCM assigned only a tiny amount of the Z20 GW type as intruding into the eastern NSA flow path, any attempt to run the MCM without the intrusion of this ancient brackish GW failed to reach an optimized solution. This may indicate that the Z20 water type constitutes a major brackish GW body that feeds the NSA along the eastern Negev flow path. The hydrochemical composition does not recognize the Z20 GW as a typical "Dead Sea brine" identified in several exploration boreholes in the northern Arava Valley (Kafri et al., 2008; Starinsky, 1974). Thus, it is feasible to assume the existence of a deep artesian, highly pressurized brackish GW reservoir yet to be explored in the Arava Rift Valley. Finally, the geological faults across the Negev Highlands serve as conduits that might explain the identified massive entries of GW into the NSA from surrounding aquifers on the way to the Arava Valley.

As for the significance of the calculated GW fluxes, the analytical accuracy of the data and the assigning of potential sources associated with specific hydrochemical and isotopic characterizations to every cell in the model might be incomplete or even erroneous, raising questions about the model's sensitivity to imprecise input data. The hydrochemical and isotopic characterizations may somewhat deviate from the values assigned in the model for the GW representing the homogeneous concentrations in each cell or of every potential source. Also, the assumptions behind the model that the GW flow pattern is precisely understood and that all the potential inflows have been identified might not be fully satisfied. The sensitivity of the MCM to possibly slight deviations from the "true" hydrochemical and isotopic data was rigorously studied (Adar et al., 1988), with the conclusion that once an optimized solution is achieved for realistic hydrochemical and isotopic compositions, the MCM provides an accurate assessment of the unknown GW fluxes.

5. Summary and conclusion

This work was inspired by the complex apparent age distribution of GW in the NSA revealed by ^{81}Kr measurements. It demonstrates a more sophisticated approach to interpreting the ^{81}Kr tracer data, which a simple closed-system GW flow model could not readily solve. Prompted by a peculiar GW age pattern and resolved by mixing cell flow modeling, this study revealed the discharge within and into the complex NSA flow system. The MCM approach identified and assessed GW fluxes from active connected sources into the NSA from the surrounding aquifers and the variations of GW fluxes in the NSA along the eastern Negev flow path. Results show that ancient GW in the NSA flows from Sinai through the eastern Negev towards the outlet south of the Dead Sea and mixes with mostly younger GW sources along its flow path. In addition, the NSA under the Negev Desert gains small, yet substantial, upward fluxes from a deep-seated, brackish artesian GW reservoir along the edge of the Arava Valley. Groundwater recharge through the calcareous Upper Cretaceous Aquifer provides younger GW to all the cells from Cell II to VII through the faults that breach the NS formations, significantly rejuvenating the GW age in the NSA. Even younger GW flows into Cell VI from the Senonian Chalk and Chert Aquifer. Therefore, these findings indicate that the Nubian Sandstone Aquifer under the Negev Desert is not entirely isolated, as reflected by the absence of a continuous trend in the spatial variation of the hydrochemical and isotopic compositions of oxygen and hydrogen and implied by the ^{81}Kr age variations without a clear trend downflow along the eastern Negev flow path. Beyond the use of water-stable isotopes, along with hydrochemical data, to qualitatively assess hydrological connections between aquifers and GW-bearing formations, the MCM approch can quantitatively estimate the flows (GW fluxes) within, into, and from the aquifer and between sub-aquifers. This article demonstrates the ability of the MCM to locate active GW fluxes from nearby water bodies and quantitatively assess the spatial distribution of GW flows to and within a complex aquifer. The results explain and support the spatial distribution and fluctuations of the water age in the aquifer as obtained from ^{81}kr, which cannot be obtained from implementing a flow model, due to the lack of hydrological information and the aquifer's hydrogeological complexity. The approach presented in this study might apply to examining recharge processes and hydraulic connectivity in other aquifers that were formerly classified as "fossil," such as the immense Nubian sandstone aquifers found in the Arabian (Jordan and Saudi Arabia) and the Western (Egypt) Deserts.

Author contributions

Betzabe Atencio (B.A.) and Roi Ram (R.R.) (equal contribution) performed the integration between the spatial distribution of the isotopic composition, hydrochemistry, and GW age, with the hydrogeology and the results from the MCM approach, and wrote the original draft. Zheng-Tian Lu (Z.T.L)(, Reika Yokochi (R.Y.), and Eilon Adar (E.A.) visualized and conceived the project from its inception: dating ancient GW with the help of krypton isotopes downstream of the aquifer to examine the hydrological significance of an irregular distribution of GW ages defined with carbon-14. E.A. fitted and adapted the MCM to the flow pattern in the aquifer and reviewed and edited the original and the final drafts. B.A., R.R., and E.A. sampled and in situ degassed the GW. R. Y. and Roland Purtschert developed and performed the in-situ extraction of dissolved gases from GW and separating krypton gas. Z.T.L. and Wei Jiang developed the methodology, measured the krypton isotopic ratios, and calculated the GW ages. Avihu Burg and R.R. incorporated the geological structures into the flow model. Yoseph Yechieli, R.R., Zeev Ronen, and E.A. assessed the hydrogeology given the hydrochemistry and isotopic distribution over the aquifer. All authors contributed, read, and approved the final manuscript.

Funding sources

Financial support for conducting the research was provided by the US-Israel Water Funding Opportunities by the University of Chicago, Argonne National Laboratory, and Ben-Gurion University of the Negev, followed by a substantial contribution made by the U.S.-Israel Binational Science Foundation (BSF; grant no. 2014351), the Israel Science Foundation (ISF; grant number no. 1068/20), and the Israel Water Authority, Ministry of Energy (grant no. 4501284811). The research has also been supported by grants from the National Secretariat of Science, Technology, and Innovation (SENACYT) of the Republic of Panama. The above funding sources selected this project based on scientific merit. They had no involvement in the study design, collection, analyses, interpretation of data, writing of the reports, or the decision to submit the article for publication.

Credit authorship contribution statement

Betzabe Atencio: . **Roi Ram:** . **Avihu Burg:** Conceptualization, Investigation. **Reika Yokochi:** Conceptualization, Methodology, Visualization, Funding acquisition, Investigation. **Yoseph Yechieli:** Conceptualization, Investigation, Methodology. **Roland Purtschert:** . **Zheng-Tian Lu:** . **Wei Jiang:** . **Zeev Ronen:** . **Eilon M. Adar:** .

Declaration of competing interest

The authors declare that they have no known competing financial interests or personal relationships that could have appeared to influence the work reported in this paper.

Data availability

Data will be made available on request.

Acknowledgments

The authors thank the following institutions and organizations for supporting and assisting the research project: the US-Israel Water Funding Opportunities by the University of Chicago, Argonne National Laboratory, and the Ben-Gurion University of the Negev; the U.S.-Israel Binational Science Foundation (BSF); the Israel Science Foundation; the Israel Water Authority, the Geological Survey of Israel, and "Mekorot," the National Water Company of Israel. Additionally, we extend our appreciation to Jake Zappala and Peter Mueller for their valuable contribution to the methodology development, performing the krypton-81 analyses, and their efforts in calculating the GW ages.

Appendix A. Supplementary data

Supplementary data to this article can be found online at https://doi.org/10.1016/j.jhydrol.2024.130631.

References

Abd El Samie, S.G., Sadek, M.A., 2001. Groundwater recharge and flow in the Lower Cretaceous Nubian Sandstone aquifer in the Sinai Peninsula, using isotopic techniques and hydrochemistry. Hydrogeol. J. 9, 378–389. https://doi.org/10.1007/s100400100140.

Abouelmagd, A., 2012. Paleoclimatic Regimes of the African Sahara Desert During Pleistocene and the Origin of Groundwater in the Nubian Sandstone Aquifer System. Western Michigan University. Ph.D. Dissertation,.

Abouelmagd, A., Sultan, M., Sturchio, N.C., Soliman, F., Rashed, M., Ahmed, M., Kehew, A.E., Milewski, A., Chouinard, K., 2014. Paleoclimate record in the Nubian Sandstone Aquifer, Sinai Peninsula. Egypt. Quat. Res. 81 (1), 158–167. https://doi.org/10.1016/j.yqres.2013.10.017.

Adar, E., Neuman, S.P., Woolhiser, D.A., 1988. Estimation of spatial recharge distribution using environmental isotopes and hydrochemical data: I. mathematical model and application to synthetic data. J. Hydrol. 97 (3–4), 251–277. https://doi.org/10.1016/0022-1694(88)90119-9.

Adar, E., Neuman, S.P., 1988. Estimation of spatial recharge distribution using environmental isotopes and hydrochemical data: II. application to aravaipa valley in southern arizona. J. Hydrol. 97 (3–4), 279–302. https://doi.org/10.1016/0022-1694(88)90120-5.

Aggarwal, P.K., Araguas-Araguas, L., Choudhry, M., van Duren, M., Froehlich, K., 2014. Lower groundwater ^{14}C age by atmospheric CO_2 uptake during sampling and analysis. Groundwater 52, 20–24. https://doi.org/10.1111/gwat.12110.

Bajracharya, K., Barry, D.A., 1994. Note on common mixing cell models. J. Hydrol. 153 (1–4), 189–214. https://doi.org/10.1016/0022-1694(94)90191-0.

Bear, J., 1979. Hydraulics of groundwater. McGraw-Hill series in water resources and environmental engineering. McGraw-Hill Inc., New York.

Burg, A., Zilberbrand, M., Yechieli, Y., 2013. Radiocarbon variability in groundwater in an extremely arid zone - the Arava Valley, Israel. Radiocarbon 55, 963–978. https://doi.org/10.1017/S0033822200058112.

Calvo, R., Gvirtzman, Z., 2013. Assessment of CO_2 storage capacity in southern Israel. Int. J. Greenh. Gas Control 14, 25–38. https://doi.org/10.1016/j.ijggc.2012.12.027.

Campana, M.F., Simpson, E.S., 1984. Groundwater residence times and discharge rates using discrete-state compartmental model and ^{14}C data. J. Hydrol. 72, 171–185. https://doi.org/10.1016/0022-1694(84)90190-2.

Dvory, N.Z., 2009. Negev and Arava Model - Implementing an operational model in the GMS version 6 interface. Israel Water Authority, Ministry of National Infrastructures. 73, pp in Hebrew.

Freeze, R.A., Cherry, J.A., 1979. Groundwater. Prentice-Hall Inc., Englewood Cliffs 7632, 604 pp.

Frieslander, U., 2000. The structure of the Dead Sea Transform emphasizing the Arava, using new geophysical data. Ph.D. Dissertation, The Hebrew University of Jerusalem, Israel (in Hebrew, English abstract).

Gat, J.R., Issar, A., 1974. Desert isotope hydrology: water sources of the sinai desert. Geochim. Cosmochim. Acta 38, 1117–1131. https://doi.org/10.1016/0016-7037(74)90008-8.

Guttman, Y., Burg, A., Lifshitz, Y., Lumelsky, S., Zukerman, H., 1999. Hydrological model for estimation of water potential in the Arava aquifers – final report. Tahal Company Ltd. Report 6127–d99.201 (In Hebrew).

Issar, A., 1979. The paleohydrology of southern Israel and its influence on the flushing of the Kurnub and 'Arad groups (Lower Cretaceous and Jurassic). J. Hydrol. 44, 289–303. https://doi.org/10.1016/0022-1694(79)90136-7.

Issar, A., 1985. Fossil water under the Sinai-Negev peninsula. Sci. Am. 253, 104–110.

Issar, A., Bein, A., Michaeli, A., 1972. On the ancient water of the Upper Nubian Sandstone aquifer in central Sinai and southern Israel. J. Hydrol. 17, 353–374. https://doi.org/10.1016/0022-1694(72)90092-3.

JICA (Japan International Cooperation Agency), 1999. South Sinai groundwater resources study in the Arab Republic of Egypt. Pacific Consultants International and Sanyu Consultants Inc., Tokyo.. Final Report 99/062.

Kafri, U., Goldman, M., Levi, E., 2008. The relationship between saline groundwater within the Arava Rift Valley in Israel and the present and ancient base levels as detected by deep geoelectromagnetic soundings. Environ. Geol. 54, 1435–1445. https://doi.org/10.1007/s00254-007-0924-2.

Kroitoru, L., 1980. The hydrogeology of the Nubian Sandstone in southern Israel. Tel Aviv University, Israel.. M.Sc. thesis (In Hebrew, English abstract).

Matthews, A.J., 2013. Application of the Mixing Cell Model to the quantification of groundwater-surface water interaction. M.Sc. thesis. University of the Free State, South Africa.

Moustafa, A.R., Khalil, M.H., 1994. Rejuvenation of the eastern Mediterranean passive continental margin in northern and central Sinai: new data from the Themed Fault. Geol. Mag. 131, 435–448. https://doi.org/10.1017/S0016756800012085.

Partington, D., Brunner, P., Simmons, C.T., Therrien, R., Werner, A.D., Dandy, G.C., Maier, H.R., 2011. A hydraulic mixing-cell method to quantify the groundwater component of streamflow within spatially distributed fully integrated surface water–groundwater flow models. Environ. Model. Soft. 26 (7), 886–898. https://doi.org/10.1016/j.envsoft.2011.02.007.

Ram, R., Burg, A., Zappala, J.C., Yokochi, R., Yechieli, Y., Purtschert, R., Jiang, W., Lu, Z.-T., Mueller, P., Bernier, R., Adar, E.M., 2020. Identifying recharge processes into a vast "fossil" aquifer based on dynamic groundwater ^{81}Kr age evolution. J. Hydrol. 587, 124946 https://doi.org/10.1016/j.jhydrol.2020.124946.

Ram, R., Burg, A., Adar, E.M., 2021a. The Nubian Sandstone Aquifer in the Sinai Peninsula and the Negev Desert. In: Kafri, U., Yechieli, Y. (Eds.), The Many Facets of Israel's Hydrogeology. Springer International Publishing, Cham, pp. 115–141. https://doi.org/10.1007/978-3-030-51148-7_9.

Ram, R., Purtschert, R., Adar, E.M., Bishof, M., Jiang, W., Lu, Z.-T., Mueller, P., Sy, A., Vockenhuber, C., Yechieli, Y., Yokochi, R., Zappala, J.C., Burg, A., 2021b. Controls on the $^{36}Cl/Cl$ input ratio of paleo-groundwater in arid environments: new evidencefrom $^{81}Kr/Kr$ data. Sci. Total Environ. 762, 144106 https://doi.org/10.1016/j.scitotenv.2020.144106.

Rosenthal, E., Zilberbrand, M., Livshitz, Y., 2007. The hydrochemical evolution of brackish groundwater in central and northern Sinai (Egypt) and in the western Negev (Israel). J. Hydrol. 337, 294–314. https://doi.org/10.1016/j.jhydrol.2007.01.042.

Shalaby, A., Embaby, A., Seiam, A., 2012. Structural constraints on the groundwater regime of the Cretaceous aquifers in Central Sinai. Egypt. J. African Earth Sci. 75, 37–56. https://doi.org/10.1016/j.jafrearsci.2012.07.007.

Starinsky, A., 1974. Relationship between Ca-chloride brines and sedimentary rocks in Israel. Ph.D. Dissertation, The Hebrew University of Jerusalem, Israel (in Hebrew, English abstract).

Tsur, Y., Park, H., Issar, A., 1989. Fossil groundwater resources as a basis for arid zone development? Int. J. Water Resour. Dev. 5, 191–201. https://doi.org/10.1080/07900628908722433.

Vengosh, A., Hening, S., Ganor, J., Mayer, B., Weyhenmeyer, C.E., Bullen, T.D., Paytan, A., 2007. New isotopic evidence for the origin of groundwater from the Nubian Sandstone Aquifer in the Negev. Israel. Appl. Geochemistry 22, 1052–1073. https://doi.org/10.1016/j.apgeochem.2007.01.005.

Wang, F., Li, Q., Liu, H., Geng, X., 2016. Quantitative analysis of groundwater recharge in an arid area. Northwest China. Water 8, 354. https://doi.org/10.3390/w8080354.

Wolfe, P., 1959. The Simplex Method for Quadratic Programming. Econometrica 27 (3), 382–398. https://doi.org/10.2307/1909468.

Woolhiser, D.A., Gardner, H.R., Olsen, S.R., 1982. Estimation of multiple inflows to a stream reach using water chemistry data. Trans. ASAE 25 (3), 616–622.

WPRP (Water Policy Reform Program), 1998. Hydrogeology of Deep Aquifers in the Western Desert and Sinai. Ministry of Public Works and Water Resources, Water Policy Reform Program, Cairo, Egypt, p. 208.

Yokochi, R., Ram, R., Zappala, J.C., Jiang, W., Adar, E., Bernier, R., Burg, A., Dayan, U., Lu, Z.-T., Mueller, P., Purtschert, R., Yechieli, Y., 2019. Radiokrypton unveils dual moisture sources of a deep desert aquifer. Proc. Natl. Acad. Sci. 116, 16222–16228. https://doi.org/10.1073/pnas.1904260116.